

# A Framework for Fluid Motion Estimation using a Constraint-Based Refinement Approach

Hirak Doshi, N. Uday Kiran

## Abstract

The goal of this paper is to formulate a general framework for fluid motion estimation using a constraint-based refinement approach. We demonstrate that for a particular choice of the constraint, our results closely approximate the continuity equation based fluid flow. This closeness is theoretically justified through a modified augmented Lagrangian method and validated numerically. Further, along with the continuity constraint, our model can include other geometric constraints as demonstrated. The mathematical well-posedness is studied in the Hilbert space setting. Moreover, a special feature of our system is the possibility of a diagonalization by the Cauchy-Riemann operator and transforming it to a diffusion process on the curl and the divergence of the flow. Using the theory of semigroups on the decoupled system, we show that our approach preserves the spatial characteristics of the divergence and the vorticities. We perform several numerical experiments and show the results on different datasets.

**Keywords.** Optical Flow, Fluid Flow, Variational Formulation, Diffusion Process, Augmented Lagrangian, Multiplicative Perturbation of the Laplacian, Evolutionary PDE.

**Mathematics Subject Classification 2020.** 35J47, 35J50, 35Q68.

## 1 Introduction

Variational models for motion estimation have always been one of the central topics in Mathematical Image Processing. Since the seminal work of Horn and Schunk [16] on the variational approach to optical flow motion estimation, many in-depth studies on this topic have been done through developing different variational models of optical flow to obtain useful insights into motion estimation (e.g. [22, 3, 15, 25]). Many of these literature works on motion estimation has been focused on the constancy assumption e.g., the brightness constancy leading to an algebraic equation, in  $(u, v)$  the motion components, called the optical flow constraint (OFC) :

$$f_\tau + f_x u + f_y v = 0, \quad (1)$$

where  $f(x, y, \tau)$  is the image sequence  $f : \Omega \times [0, \infty) \rightarrow \mathbb{R}$  for an open bounded set  $\Omega \subset \mathbb{R}^2$ ,  $(x, y)$  are the spatial coordinates and  $\tau$  is the time variable. However, constancy assumptions can't reflect the reality of actual motion because deformation

effects of fluid, illumination variations, perspective changes, poor contrast etc. would directly affect the important motion parameters. For this reason, physics-dependent motion estimation algorithms have been widely investigated.

### 1.1 Related Work

A relatively recent and representative work of Corpetti et.al. [7], in which fluid mechanics was used to extending the optical flow estimation, and accurate dense motion fields were obtained. This method includes an image-based integrated version of the continuity equation from fluid dynamics. Since then there has been a lot of attention on studying the physics-based motion estimation. Estimates on the conservation of mass for a fluid in a digital image sequence was discussed by Wildes et.al. [26]. They model the image intensity as an average of the object density and consider the incident light parallel to the  $z$ -axis such that the 2D projection of the image intensity is captured as

$$f(x, y, \tau) = \int_{z_1}^{z_2} \rho(x, y, z, \tau) dz.$$

Further using fluid mechanics models Liu et.al. [24] provided a rigorous framework for fluid flow by deriving the projected-motion equations. Here the optical flow is proportional to the path-averaged velocity of fluid or particles weighted with a relevant field quantity. Luttmann et.al. [19] computed the potential (resp. stream) function directly by assuming that the flow estimate is the gradient of a potential function (resp. symplectic gradient of a stream function). To overcome the limitations of the global smoothness regularization for fluid motion estimation, Corpetti et.al [8] proposed a second-order div-curl regularization for a better estimation of intrinsic flow structures. A detailed account of various works in the fluid flow based on physics is given in [14]. Here the authors observed a physical meaning associated with the terms of the continuity equation (CEC) :

$$\underbrace{f_\tau + f_x u + f_y v}_{\text{(a)}} + \underbrace{f(u_x + v_y)}_{\text{(b)}} = 0; \quad (2)$$

**(a)** corresponds to the brightness constancy given in (1) and **(b)** is the non-conservation term due to loss of particles. Furthermore, a divergence-free approximation of the equation (2) could be obtained by setting the term **(b)** to zero. It is thus natural to study the effect of the term **(b)** in extracting the inherent fluid properties of the flow.

## 1.2 Our Contribution

In the current work our goal is to understand and develop a generic physics-based framework for fluid motion estimation for capturing intrinsic spatial characteristics and vorticities. To achieve this goal, we use a constraint-based refinement approach. The first requirement is that of an initial flow estimate  $(u_0, v_0)$  which obeys the classical optical flow principles like the brightness constancy and pixel correspondence. This estimate may not be able to capture the underlying geometric features of the fluid flow. The main idea is to perform a refinement over this initialized flow to capture precise flow structures driven by additional constraints specific to applications. To be precise, given an initial field  $(u_0, v_0)$  obtained by the brightness constancy based optical flow, we consider the following image driven evolutionary PDE model to modify the flow:

$$\left\{ \begin{array}{l} \frac{\partial u}{\partial t} = \Delta u + a_0 \frac{\partial}{\partial x} [\phi(f)(u_x + v_y)] \text{ in } \Omega \times (0, \infty), \\ \frac{\partial v}{\partial t} = \Delta v + a_0 \frac{\partial}{\partial y} [\phi(f)(u_x + v_y)] \text{ in } \Omega \times (0, \infty), \\ u(x, y, 0) = u_0 \text{ in } \Omega, \\ v(x, y, 0) = v_0 \text{ in } \Omega, \\ u = 0 \text{ on } \partial\Omega \times (0, \infty), \\ v = 0 \text{ on } \partial\Omega \times (0, \infty), \end{array} \right. \quad (3)$$

where  $a_0$  is a positive constant and the function  $\phi$  is image-dependent weight term. As a concrete example we choose the initial estimate coming from the Horn and Schunck model [16]. It is well-known that this model is not well-suited for fluid motion estimation. In fact the global smoothness regularization damps both the divergence and vorticity of the motion field. We will show in particular how this model can be adapted and refined through our approach. Since there is no motion at the flow boundaries, it is thus natural to work with homogeneous Dirichlet boundary conditions. A special feature of our model (3) is the diagonalization by the Cauchy-Riemann operator to obtain an implicit diffusion process

$$\frac{\partial \xi}{\partial t} = \Delta \xi \quad \text{and} \quad \frac{\partial \zeta}{\partial t} = \Delta (k\zeta), \quad (4)$$

where  $\xi := u_y - v_x$  is the curl and  $\zeta := u_x + v_y$  is the divergence of the flow and  $k = 1 + a_0\phi(f)$  is a multiplicative factor. Here the diffusion process is image dependent as a multiplicative perturbation of the Laplacian on the divergence; thereby leading to a reinterpretation of the continuity model as a transport phenomenon induced as “diffusive fluxes” expressed as functions of gradient quantities. In physics, a

similar diffusion phenomenon is observed for the gradient quantities for the fluid flow of ideal gases and plasmas in [23]. Moreover, in [18] the authors observe a path-averaging behaviour of the velocities which further justifies the underlying a diffusive behaviour.

The incompressibility condition implies that the density remains constant within a parcel of fluid that moves with the flow velocity. Even compressible flows can be locally modelled as an incompressible flow. The OFC can be viewed as a divergence-free approximation of the CEC based model (although this view is not exact, in our algorithm we start with this approximation), see [18, 6]. This is the starting point of our discussion. Having obtained a crude approximation from the Horn and Schunck optical flow in the next phase we obtain a refinement by choosing specific additional constraints. The main advantage of our method is firstly from a theoretical point of view it provides us with an evolutionary PDE setup which allows a rigorous mathematical framework for the well-posedness discussion. Secondly, due to the semigroup approach, we can have a simpler analysis and also obtain faster convergence of the solution in our scheme. A modified Bounded Constraint Algorithm [20] is employed to show the convergence of the dual variable  $\lambda$  introduced by the augmented Lagrangian formulation theoretically. The inner iterations of the algorithm use the contractive semigroup of the elliptic term. This approach thus allows us to build a quantitative connection between the optical flow and the fluid flow for various flow visualizations which is often a key problem.

The organization of the paper is as follows. Section (2) starts with the description of our variational formulation. Here we discuss the mathematical well-posedness in the Hilbert space setting and also show how the system of equations lead to a diagonalization by the Cauchy-Riemann operator leading to a diffusion process on the divergence and a multiplicative perturbation of the laplacian of the curl of the flow. In Section (3) we show how for a particular choice of additional constraints, our model closely approximate the continuity equation model using a modified augmented Lagrangian formulation. We also employ the Bounded Constraint Algorithm to show the numerical convergence of the Uzawa iterates. Finally, in Section (4) we show our results on different datasets.

## 2 Mathematical Framework

### 2.1 Description of the Model

Our main objective is to obtain a refinement of a flow field preserving certain intrinsic spatial characteristics. As a concrete example, we choose to refine the Horn and Schunck optical flow [16]. The main advantage of this formulation is the mathematical well-posedness [22]. Even though it is well-known that this model is not adequate for problems corresponding to fluid flow visualization [8, 7, 17] nevertheless, it is a reasonable starting point for pixel correspondence even for fluid flow [17].

With this background, we propose the following formulation

$$J_R(\mathbf{u}) = \beta \int_{\Omega} \phi(f) \psi(\nabla \mathbf{u}) + \alpha \int_{\Omega} \{|\nabla u|^2 + |\nabla v|^2\}, \quad (5)$$

where the constants  $\alpha, \beta$  are weight parameters, the function  $\psi$  depends on the components of the flow and its derivatives which essentially captures the underlying geometric structures and the function  $\phi$  corresponds to an image-dependent weight term. A few possible combinations are summarized in the following table:

$\phi(f)$	$\psi(\nabla \mathbf{u})$	Nature of the model
$f^2$	$(\nabla \cdot \mathbf{u})^2$	Anisotropic, image-driven, penalizing divergence of the flow
1	$(\nabla \cdot \mathbf{u})^2$	Isotropic, flow-driven, penalizing divergence of the flow
$f^2$	$(\nabla_H \cdot \mathbf{u})^2$	Anisotropic, image-driven, penalizing curl of the flow
1	$(\nabla_H \cdot \mathbf{u})^2$	Isotropic, flow-driven, penalizing curl of the flow

Table 1: Some choices for the functions  $\phi$  and  $\psi$

As seen from the table, the function  $\phi$  dictates whether the refinement process is image-driven or flow-driven. When  $\phi(f) = 1$ , there is no influence of the image data on the additional constraint. As a result the refinement process is completely flow-driven. We assume that both the functions  $\phi$  and  $\psi$  are real-valued smooth functions. Moreover, we assume  $\phi(f)$  to be a monotone increasing function. The first term of  $J_R(\mathbf{u})$  captures the non-conservation term that violate the constancy assumptions and the second term is the  $L^2$  regularization which governs the diffusion phenomena. To show the closeness of our model to the continuity model we will subsequently consider a constrained-minimization problem where the constraint governs the apriori ‘divergence-free’ estimate for the pixel correspondence. The rationale for the choice of the constraint will be discussed later. In the current work we particularly focus on the case where  $\psi = (\nabla \cdot \mathbf{u})^2$ , i.e. where the function  $\psi$  penalizes the divergence of the flow. In this case the refinement functional becomes

$$J_R(\mathbf{u}) = \beta \int_{\Omega} \phi(f) (\nabla \cdot \mathbf{u})^2 + \alpha \int_{\Omega} \{|\nabla u|^2 + |\nabla v|^2\}. \quad (6)$$

Here we would also like to mention that the regularization term is not limited to global smoothness. One can suitably adopt a different regularization scheme depending on the application.

## 2.2 Additional Constraint penalizing the Curl of the Flow

Our refinement process leads to a general framework for fluid motion estimation which can be easily adapted to specific application-dependent problems. The choice of additional constraints play a crucial role in determining which aspects of the

flow are to be captured. In Table (1) we have suggested two such choices for  $\psi$ , one penalizing the divergence of the flow and the other penalizing the curl. The operator  $\nabla_H := (\partial_y, -\partial_x)$  is called the orthogonal gradient also referred to as the symplectic gradient in the literature [19]. This particular constraint captures the rotational aspects of the flow much better than the divergence one. A detailed study involving this constraint will be discussed in a forthcoming paper. However a unique feature of our formulation involving this constraint alongwith  $\phi(f) = 1$  (fourth combination from Table (1)) will be demonstrated later in the results section where we will show that for the Jupiter's white oval sequence the flow-driven refinement involving the curl-penalization term actually compares to the continuity equation very closely even without implicitly assuming the illumination correction which is a necessary assumption for this sequence (see [17]).

### 2.3 Diagonalization of the System

In this section we will show that the system (3) can be diagonalized by an application of Cauchy-Riemann operator. This special feature is intriguing as well as of great advantage for later analysis. Let us first rewrite the system (3) as

$$\frac{\partial \mathbf{u}}{\partial t} = A\mathbf{u}, \quad (7)$$

where

$$\frac{\partial \mathbf{u}}{\partial t} = \begin{bmatrix} \frac{\partial u}{\partial t} \\ \frac{\partial v}{\partial t} \end{bmatrix}, \quad A\mathbf{u} = \begin{bmatrix} \Delta u + a_0 \frac{\partial}{\partial x} [\phi(f)(u_x + v_y)] \\ \Delta v + a_0 \frac{\partial}{\partial y} [\phi(f)(u_x + v_y)] \end{bmatrix}.$$

As we are in the Sobolev setting, the derivatives are taken in a distributional sense. Thus, a key observation is that the order of derivatives can be interchanged. Let us denote by  $R$  the Cauchy-Riemann operator matrix

$$R = \begin{bmatrix} \partial_y & -\partial_x \\ \partial_x & \partial_y \end{bmatrix}.$$

Acting  $R$  on both sides of (7) leads to

$$R\left(\frac{\partial \mathbf{u}}{\partial t}\right) = RA\mathbf{u}.$$

This leads to the following transformation of the original coupled system

$$\begin{bmatrix} \partial_y & -\partial_x \\ \partial_x & \partial_y \end{bmatrix} \begin{bmatrix} \frac{\partial u}{\partial t} \\ \frac{\partial v}{\partial t} \end{bmatrix} = \begin{bmatrix} \partial_y & -\partial_x \\ \partial_x & \partial_y \end{bmatrix} \begin{bmatrix} \Delta u + a_0 \frac{\partial}{\partial x} [\phi(f)(u_x + v_y)] \\ \Delta v + a_0 \frac{\partial}{\partial y} [\phi(f)(u_x + v_y)] \end{bmatrix}$$

$$= \begin{bmatrix} \Delta & 0 \\ 0 & \Delta \circ k \end{bmatrix} \begin{bmatrix} \partial_y & -\partial_x \\ \partial_x & \partial_y \end{bmatrix} \begin{bmatrix} u \\ v \end{bmatrix},$$

where with a slight abuse of notation we denote  $k$  for the function  $1 + a_0\phi(f)$  and for the multiplicative operator  $x \mapsto kx$ . Since  $\phi$  is a bounded function and  $a_0 > 0$ , the multiplicative term  $k$  is bounded and strictly positive. We have thus obtained the following decoupling:

$$\frac{\partial}{\partial t}(R\mathbf{u}) = DR\mathbf{u}, \quad (8)$$

where

$$D = \begin{bmatrix} \Delta & 0 \\ 0 & \Delta \circ k \end{bmatrix}, \quad R = \begin{bmatrix} \partial_y & -\partial_x \\ \partial_x & \partial_y \end{bmatrix}.$$

The application of the Cauchy-Riemann operator  $R$  on the system has resulted in the following relation

$$D = RAR^{-1}.$$

The operator  $A$  has been diagonalized by the matrix  $R$ . The decoupled system (8) thus takes the following form:

$$\begin{cases} \frac{\partial \xi}{\partial t} = \Delta \xi, \\ \frac{\partial \zeta}{\partial t} = \Delta(k\zeta), \end{cases} \quad (9)$$

where  $\xi := u_y - v_x$  is the curl and  $\zeta := u_x + v_y$  is the divergence of the flow and  $k = 1 + a_0\phi(f)$  is a multiplicative factor.

## 2.4 Multiplicative Perturbation of the Laplacian

Let us consider the divergence equation from (9)

$$\frac{\partial \zeta}{\partial t} = \Delta(k\zeta), \quad (10)$$

where  $k = 1 + a_0\phi(f)$ . We make a change of variable  $\eta = k\zeta$ . This transformation leads to the equation:

$$\frac{\partial \eta}{\partial t} = k\Delta\eta. \quad (11)$$

The operator  $k\Delta$  is the multiplicative perturbation of the laplacian. It arises in many physical phenomena e.g. in the theory of wave propagation in non-homogeneous media. The operator has been studied in appropriate weighted function spaces see [11, 2]. In our case the multiplicative perturbation  $k\Delta$  leads to an image driven perturbation because of the  $k$  factor which depends on the image  $f$ . The authors in

[2] derive an approximation for the kernel of the associated semigroups by positive linear integral operators

$$G_m(f)(x) = \left( \frac{m}{4\pi k(x)} \right)^{n/2} \int_{\mathbb{R}^n} f(y) \exp \left( - \frac{m}{4k(x)} |x - y|^2 \right) dy. \quad (12)$$

Using the above kernel one can design an appropriate stencil for convolution. It is also interesting to note that the stencil size varies with respect to the image intensity. This aspect we will discuss in a forthcoming paper. Let us now consider the Gaussian kernel associated with the operator  $k\Delta$

$$G_k(x, t) := \frac{1}{4\pi k(x)t} \exp \left( - \frac{|x|^2}{4k(x)t} \right).$$

The perturbation  $k$  plays an important role in controlling the rate of diffusion. If  $k$  is large then the Gaussian becomes broader and shorter and if it is small then the Gaussian is thinner and taller. Using the boundedness of  $k$ , i.e.  $a_1 \leq k(x) \leq a_2, a_i > 0, i = 1, 2$ , we can show the following bound on  $G_k(x, t)$ .

**Lemma 1.** Let  $n = 2$ . Then

$$\|G_k(x, t)\|_p \leq C_k t^{(1-p)/p},$$

where the constant

$$C_k = \frac{1}{4\pi a_1} \left( \frac{4\pi a_2}{p} \right)^{1/p}.$$

## 2.5 Wellposedness and Regularity

Let us now consider the abstract IVP associated with the first equation in (9):

$$\begin{cases} \frac{d\xi}{dt} + A_1 \xi = 0 \text{ on } [0, \infty), \\ \xi(0) = \xi_0 \in L^2(\Omega). \end{cases} \quad (13)$$

where the initial data

$$\xi_0 = \partial_y u_0 - \partial_x v_0,$$

and  $(u_0, v_0)$  is the Horn and Schunck optical flow. Here  $A_1 : D(A_1) \rightarrow \mathcal{H}_1$  is an (unbounded) operator

$$\begin{cases} D(A_1) = \{\xi \in H^2(\Omega) \cap H_0^1(\Omega) : A_1 \xi \in L^2(\Omega)\}, \\ \mathcal{H}_1 = L^2(\Omega), \\ A_1 \xi := -\Delta \xi. \end{cases}$$



The operator  $A_1$  is maximal monotone and symmetric. Hence it is self adjoint. For the well-posedness of the problem (13) we refer to (Theorem 7.7 and 10.1 in [5]). Similarly, the abstract IVP for the second equation becomes

$$\begin{cases} \frac{d\eta}{dt} + A_2\eta = 0 \text{ on } [0, \infty), \\ \eta(0) = \eta_0 \in L^2(\Omega). \end{cases} \quad (14)$$

where the initial data

$$\eta_0 = k(\partial_x u_0 + \partial_y v_0),$$

is the weighted divergence of the Horn and Schunck optical flow. Here  $A_2 : D(A_2) \rightarrow \mathcal{H}_2$  is the (unbounded) operator

$$\begin{cases} D(A_2) = \{\eta \in H^2(\Omega) \cap (H_0^1)_k(\Omega) : A_2\eta \in L_k^2(\Omega)\}, \\ \mathcal{H}_2 = L_k^2(\Omega), \\ A_2\eta = -k\Delta\eta. \end{cases}$$

Also  $\eta_0 \in L^2(\Omega)$ . Here the operator  $k\Delta$  is a multiplicative perturbation of the laplacian where  $k$  is bounded and strictly positive since  $\phi$  is a monotone increasing function. The problem will be studied in weighted Sobolev space  $\mathcal{H}_2$  following a similar approach as in [11]. The space  $\mathcal{H}_2$  is a Hilbert space equipped with the inner product

$$\langle w_1, w_2 \rangle_{\mathcal{H}_2} := \int_{\Omega} \frac{1}{k} w_1 w_2 \, dx$$

and the norm

$$\|w\|_{\mathcal{H}_2}^2 = \int_{\Omega} \frac{1}{k} |w|^2 \, dx.$$

Similarly the Hilbert space  $\mathcal{H}_3 := (H_0^1)_k(\Omega)$  has the norm [11]

$$\|w\|_{\mathcal{H}_3}^2 := \|w\|_{\mathcal{H}_2}^2 + \|\nabla w\|_{\mathcal{H}_1}^2 = \int_{\Omega} \left( \frac{1}{k} |w|^2 + |\nabla w|^2 \right).$$

The operator  $A_2$  is symmetric and maximal monotone. It is also interesting to note that in our context the weight term  $k$  in  $\mathcal{H}_2$  is actually dependent on the image  $f$  - bringing in an anisotropy into the discussion. Thus  $\mathcal{H}_2$  is an image dependent Sobolev space. When  $\phi(f)$  is a constant function, i.e. the case where the refinement is independent of the image, the norms  $\|\cdot\|_{\mathcal{H}_1}$  and  $\|\cdot\|_{\mathcal{H}_2}$  coincide upto a constant. In our context, as the values of the image are bounded,  $k$  is a bounded function. Also in the pre-processing stage since the images are smoothened with a Gaussian filter we can further assume that  $k$  is smooth. We will prove a result on the regularity of the solution for any non-zero time in the diffusion process.

**Theorem 1.** Let  $\eta_0 \in \mathcal{H}_1$ . Then the solution of the problem (14) satisfies

$$\eta \in C^1((0, \infty), \mathcal{H}_2) \cap C([0, \infty), H^2(\Omega) \cap \mathcal{H}_3).$$

For any  $\epsilon > 0$  we also have

$$\eta \in C^\infty([\epsilon, \infty) \times \overline{\Omega}). \quad (15)$$

Moreover,  $\eta \in L^2((0, \infty), \mathcal{H}_3)$ , and

$$\frac{1}{2} \|\eta(T)\|_{\mathcal{H}_1}^2 + \int_0^T \|\nabla \eta(t)\|_{\mathcal{H}_1}^2 dt = \frac{1}{2} \|\eta_0\|_{\mathcal{H}_2}^2 \quad (16)$$

holds for  $T > 0$ .

*Proof.* We only show the energy estimates as the remaining part of the proof follows very closely to the proof of theorem 10.1 in [5]. By Lemma ?? and ?? the operator  $A_2$  is symmetric and maximal monotone. Hence it is self-adjoint. Therefore, by Theorem 7.7 in [5], we have

$$\eta \in C^1((0, \infty), \mathcal{H}_2) \cap C([0, \infty), H^2(\Omega) \cap \mathcal{H}_3).$$

Define  $\sigma(t) = \frac{1}{2} \|\eta(t)\|_{\mathcal{H}_2}^2$ . Since  $\eta \in C^1((0, \infty), \mathcal{H}_2)$  it is clear that  $\sigma$  is  $C^1$  on  $(0, \infty)$ . Therefore

$$\begin{aligned} \sigma'(t) &= \left\langle \eta(t), \frac{d\eta}{dt}(t) \right\rangle_{\mathcal{H}_2} \\ &= \left\langle \eta(t), k\Delta\eta \right\rangle_{\mathcal{H}_2} \\ &= \left\langle \eta(t), \Delta\eta \right\rangle_{\mathcal{H}_1} \\ &= -\|\nabla\eta(t)\|_{\mathcal{H}_1}^2. \end{aligned}$$

Integrating from  $\epsilon$  to  $T$  where  $0 < \epsilon < T < \infty$  we get

$$\sigma(T) - \sigma(\epsilon) = - \int_\epsilon^T \|\nabla\eta(t)\|_{\mathcal{H}_1}^2 dt.$$

Again as  $\eta \in C((0, \infty), \mathcal{H}_2(\Omega))$  we have  $\sigma(\epsilon) \rightarrow \sigma(0) = \frac{1}{2} \|\eta_0\|_{\mathcal{H}_2}^2$  as  $\epsilon \rightarrow 0$ . Therefore in the limiting case we obtain

$$\sigma(T) + \int_0^T \|\nabla\eta(t)\|_{\mathcal{H}_1}^2 dt = \frac{1}{2} \|\eta_0\|_{\mathcal{H}_2}^2,$$

and (16) holds. Integrating the Hilbert space  $(H_0^1)_k(\Omega)$  norm defined above from 0

to  $T$  we get

$$\begin{aligned}
\int_0^T \|\eta(t)\|_{(H_0^1)^k}^2 dt &= \int_0^T \|\eta(t)\|_{\mathcal{H}_2}^2 dt + \int_0^T \|\nabla \eta(t)\|_{\mathcal{H}_1}^2 dt \\
&= 2 \int_0^T \sigma(t) dt + \int_0^T \|\nabla \eta(t)\|_{\mathcal{H}_1}^2 dt \\
&\leq 2 \int_0^T \sigma(t) dt + \frac{1}{2} \|\eta_0\|_{\mathcal{H}_2}^2.
\end{aligned}$$

This shows that

$$\eta \in L^2((0, \infty), \mathcal{H}_3).$$

□

### 3 A Special Case: Approximating the Continuity Equation Model

In this section we show that for a specific choice of the additional constraint  $\phi(f) = f^2$ ,  $\psi = (\nabla \cdot \mathbf{u})^2$ , our model closely approximates the CEC based model. We justify this theoretically using the modified augmented Lagrangian framework.

#### 3.1 The Augmented Lagrangian Framework

Let  $\mathcal{V} = H^1(\Omega) \times H^1(\Omega)$  and  $\mathcal{H} = L^2(\Omega)$  denote the Hilbert spaces with the respective norms  $\|\cdot\|_{\mathcal{V}}$ ,  $\|\cdot\|_{\mathcal{H}}$ . For simplicity, we fix  $\alpha = \beta = 1$ . Recall that our refinement model evolves over an initial estimate for which the pixel correspondence problem is already solved upto a certain level. This means that the optical flow constraint (OFC) is satisfied by the flow estimate. Taking this into account we recast the variational problem to a constrained minimization problem:

$$\min_{\mathbf{v}} J_R(\mathbf{v}) = \beta \int_{\Omega} f^2 (\nabla \cdot \mathbf{v})^2 + \alpha_1 \int_{\Omega} (|\nabla \bar{u}|^2 + |\nabla \bar{v}|^2), \quad (17)$$

subject to the constraint

$$B\mathbf{v} := \nabla f \cdot \mathbf{v} = -f_t =: c. \quad (18)$$

where  $\mu_R > 0$  and  $\lambda_1 \in \mathcal{H}$  is the Lagrange multiplier. Since OFC is a divergence-free approximation of the continuity equation data term, a similar constrained minimization problem can be considered:

$$\min_{\mathbf{v}} J_C(\mathbf{v}) = \int_{\Omega} (f_t + \nabla \cdot (f\mathbf{v}))^2 + \alpha_2 \int_{\Omega} (|\nabla \bar{u}|^2 + |\nabla \bar{v}|^2), \quad (19)$$

subject to the constraint

$$B\mathbf{v} = c. \quad (20)$$

The associated augmented lagrangian for the problem (19)-(20) will then be written as:

$$\mathcal{L}_{\mu_C}(\mathbf{v}, \lambda_1) = J_C(\mathbf{v}) + \frac{\mu_C}{2} \|B\mathbf{v} - c\|^2 + \langle \lambda_1, B\mathbf{v} - c \rangle. \quad (21)$$

**Definition 1.** A point  $(\mathbf{u}, \lambda)$  is said to be a saddle point of (21) if

$$\mathcal{L}_{\mu_C}(\mathbf{u}, \lambda_1) \leq \mathcal{L}_{\mu_C}(\mathbf{u}, \lambda) \leq \mathcal{L}_{\mu_C}(\mathbf{v}, \lambda) \quad \forall (\mathbf{v}, \lambda_1) \in \mathcal{V} \times \mathcal{H}. \quad (22)$$

To show the equivalence of the two models we will show that the saddle point of (21) is also a saddle point of (??). Let us first note the following relation:

$$J_C(\mathbf{u}) = J_{\text{HS}}(\mathbf{u}) + J_R(\mathbf{u}) + K(\mathbf{u}),$$

where  $J_{\text{HS}}$  denotes the Horn and Schunck functional and

$$K(\mathbf{u}) = 2 \int_{\Omega} (B\mathbf{u} - c)(f\nabla \cdot \mathbf{u}).$$

By the Cauchy-Schwarz inequality we have  $|K(\mathbf{u})|^2 \leq 2\|B\mathbf{u} - c\|_{L^2}^2 \|f\nabla \cdot \mathbf{u}\|_{L^2}^2$ . Thus,

$$J_C(\mathbf{u}) = J_R(\mathbf{u}) + O(\sqrt{\epsilon}) \quad \text{whenever} \quad \|B\mathbf{u} - c\|_{L^2} = O(\epsilon). \quad (23)$$

Heuristically arguing, we can take motivation from (23) and adopt a two phase strategy where we first determine the minimizer of  $J_{\text{HS}}$  and use this minimizer as an initial condition in the evolutionary PDE associated with (5). Although our model is not derived by a rigorous fluid mechanics, we still demonstrate that our results closely approximate the physics based models for this particular choice of the functions  $\phi$  and  $\psi$ . The first step is to show the equivalence of the variational problem with the associated saddle point problem, see [13, Chapter 3] for further discussions.

**Lemma 2.**  $(\mathbf{u}, \lambda)$  is a saddle point of (21) iff  $\mathbf{u}$  solves the variational problem (19)-(20).

Observe that the augmented Lagrangian (21) can be reformulated as

$$\mathcal{L}_{\mu_C}(\mathbf{v}, \lambda_1) = J_R(\mathbf{v}) + \frac{\mu_C}{2} \|B\mathbf{v} - c\|^2 + \langle \lambda_1 + 2f\nabla \cdot \mathbf{v}, B\mathbf{v} - c \rangle. \quad (24)$$

The parameters  $\mu_C, \mu_R$  can be chosen as large as necessary. The lagrange multiplier  $\lambda_1$  which acts as a dual variable is obtained by the Uzawa iteration

$$\lambda_1^{(n+1)} = \lambda_1^{(n)} + 2fd^{(n)} + \rho^{(n)}(B\mathbf{v}^{(n)} - c), \quad (25)$$

where  $d^{(n)} = \nabla \cdot \mathbf{v}^{(n)}$  and  $\rho^{(n)}$  is a tuning parameter. To show the equivalence of the two unconstrained optimization problems it is necessary that the Lagrange

multipliers  $\{\lambda_1^{(n)}\}$  converge. To show this fact we rely upon the techniques of bounded constraint algorithm, see [20, Chapter 17] for more details.

### 3.2 The Bounded Constraint Algorithm

The starting point is the crude pixel correspondence obtained from the Horn and Schunck optical flow  $\mathbf{v}^{(0)}$  obtained within a tolerance limit  $\delta_{\text{HS}}$  prescribed by Liu-Shen [18]. Observe that when the optical flow constraint is exactly satisfied then the formulations (17) and (19) coincide. However in reality due to numerical errors and approximations, the constraints are never exactly met. Thus it is natural to look at the equality constraint  $B\mathbf{u} = c$  as a bounded constraint  $\|B\mathbf{u} - c\|_{\mathcal{H}} \leq \epsilon_1^{(n)}$  where  $\epsilon_1^{(n)}$  is a threshold parameter.

---

**Algorithm 1** Bounded Constraint Algorithm

---

```

1: Set  $\lambda^{(0)}, \rho^{(0)}$ . Choose  $\epsilon_1^{(0)}, \epsilon_2^{(0)}$ .
2: Obtain initial HS optical flow  $\mathbf{v}^{(0)}$ 
3: for  $n = 1, 2, \dots$  until convergence do
4:   update  $\mathbf{v}^{(n)}, d^{(n)}$ 
5:   if  $\|B\mathbf{v}^{(n)} - c\|_{\mathcal{H}} \leq \max\{\epsilon_1^{(n)}, 2\delta_{\text{HS}}\}$ 
6:     if  $\|fd^{(n)}\|_{\mathcal{H}} \leq \epsilon_2^{(n)}$ 
7:       break;
8:     else
9:       update  $\lambda_1^{(n)}$  by (25)
10:       $\rho^{(n+1)} \leftarrow \rho^{(n)}$ 
11:      tighten tolerances  $\epsilon_1^{(n+1)}, \epsilon_2^{(n+1)}$ 
12:   else
13:     update  $B\mathbf{v}^{(n)} - c$ 
14:      $\lambda^{(n+1)} \leftarrow \lambda^{(n)}$ 
15:      $\rho^{(n+1)} \leftarrow 100\rho^{(n)}$ 
16:     tighten tolerances  $\epsilon_1^{(n+1)}, \epsilon_2^{(n+1)}$ 

```

---

The algorithm can be viewed in two phases where: in the first phase, it is purely diffusion while in the second phase it is the bounded constraint which in turn approximates the continuity equation constraint. This happens because a part of the OFC is already embedded in the CEC. This relaxation is allowed so that we do not move too far away from the constraint and to ensure that the tolerance  $\epsilon_1^{(n)}$  doesn't become too small.

### 3.3 Description of the Bounded Constraint Algorithm

Since the functionals in our work make it convenient for an efficient implementation of the augmented Lagrangian scheme we have lesser new variables. Based on the augmented Lagrangian scheme, the Bounded Constraint Algorithm (1) has outer and inner iterations. At the outer iterations, we formulate the modified augmented Lagrangian function and initialize the subproblem. The rest of the steps in the

outer iterations check for convergence and update the penalty parameter. The inner iterations solve the subproblem and update the lagrange multiplier.

At the initialization step, the initial Horn and Schunck (HS) estimate is obtained  $\mathbf{v}^{(0)}$ . The updates  $\mathbf{v}^{(n)}$  at step 4 are obtained by discretizing the Euler-Langrange equations:

$$\mathbf{P}\mathbf{v}^{(n+1)} = \mathbf{b}\mathbf{v}^{(n)}, \quad (26)$$

where

$$\mathbf{P} := \begin{bmatrix} \alpha + \frac{2\beta f^2}{\Delta x^2} & 0 \\ 0 & \alpha + \frac{2\beta f^2}{\Delta y^2} \end{bmatrix}, \quad \mathbf{b}\mathbf{v}^{(n)} = \begin{bmatrix} \alpha(M * u^{(n)}) + \beta \frac{\partial}{\partial x}[f^2 d^{(n)}] \\ \alpha(M * v^{(n)}) + \beta \frac{\partial}{\partial y}[f^2 d^{(n)}] \end{bmatrix}, \quad (27)$$

and  $M$  is the nine point approximation stencil of the laplacian.  $d^{(n)}$  is updated by the relation

$$d^{(n)} = S(t)d^{(n-1)},$$

where the map  $S(t) : u_0 \mapsto u(t) := G_k(\cdot, t) * u_0$  form a linear, continuous semigroup of contractions in  $\mathcal{H}$ ,  $G_k$  is the diffusion kernel associated with the operator  $k\Delta$ . This semigroup structure allows the process to preserve the spatial characteristics of the divergence and the vorticities.

The convergence criteria mentioned in steps 5 and 6 are checked subsequently. If both the criteria are satisfied then the required approximation is met and the algorithm terminates. If step 6 is not satisfied then we enter the inner iterations and run through steps 9 to 11 where the Lagrange multiplier  $\lambda_1$  is updated while the penalty parameter  $\mu_C$  is not modified.

The outer iteration steps 13 to 16 are executed when the convergence criteria in step 5 fail. In this case, first, the optical flow constraint is updated. Then, to preserve the convergence and to ensure no occurrence spurious updates happen, the Lagrange multiplier is assigned the value from the previous iteration. However, in our case as the bounded constraint being a divergence-free approximation of the continuity model and by the continuity of the semigroup operators on the Sobolev space, the penalty parameter will be reasonably small.

### 3.4 Convergence of the Uzawa Iterates

So far we have discussed how the modified augmented Lagrangian formulation is employed to show the equivallence of the two saddle point problems using the techniques of the Bounded Constraint Algorithm. The discussion is complete only when we prove the convergence of the Uzawa iterates (25). Using the Bounded Constraint Algorithm and the decoupling principle we show the following.

**Lemma 3.** The Uzawa iterates can be shown to satisfy the bounds

$$\|\lambda_1^{(n+1)} - \lambda_1^{(0)}\|_{\mathcal{H}} \leq 2M_1 \|f\|_{L^\infty} \|d^{(0)}\|_{\mathcal{H}} + r$$

where

$$r = \max \left\{ \frac{\pi^2}{6} m C M, 2\delta_{\text{HS}} \right\}.$$

*Proof.* Set  $n = i$  in Equation (25)

$$\lambda_1^{(i+1)} - \lambda_1^{(i)} = 2f d^{(i)} + \rho^{(i)}(B\mathbf{v}^{(i)} - c), \quad 1 \leq i \leq n.$$

Adding the  $n$  equations we obtain

$$\begin{aligned} \lambda_1^{(n+1)} - \lambda_1^{(0)} &= 2f[d^{(n)} + \dots + d^{(0)}] + \rho^{(n)}(B\mathbf{v}^{(n)} - c) + \dots + \rho^{(0)}(B\mathbf{v}^{(0)} - c) \\ &= 2f[S(t)^n d^{(0)} + \dots + d^{(0)}] + \rho^{(n)}(B\mathbf{v}^{(n)} - c) + \dots + \rho^{(0)}(B\mathbf{v}^{(0)} - c). \end{aligned}$$

Therefore

$$\lambda_1^{(n+1)} - \lambda_1^{(0)} = 2f \left[ \sum_{i=0}^n S(t)^i \right] d^{(0)} + \sum_{i=0}^n \rho^{(i)}(B\mathbf{v}^{(i)} - c).$$

Hence

$$\|\lambda_1^{(n+1)} - \lambda_1^{(0)}\|_{\mathcal{H}} \leq 2\|f\|_{L^\infty} \left| \left[ \sum_{i=0}^n S(t)^i \right] d^{(0)} \right| + \sum_{i=0}^n |\rho^{(i)}| \|B\mathbf{v}^{(i)} - c\|_{\mathcal{H}}. \quad (28)$$

Let us first consider the second sum in (28). Following the algorithm we note that  $\|B\mathbf{v}^{(n)} - c\|_{\mathcal{H}} \leq C\epsilon_1^{(n)}$ . Since the tolerance limit  $\epsilon_1^{(n)}$  is tightened after every update, there exists a  $N$  such that for  $n > N$  we can choose a  $M > 0$  such that  $\epsilon_1^{(n)} \leq M/(n+1)^2$  as long as  $\epsilon_1^{(n)} > 2\delta_{\text{HS}}$ . Thus

$$\|B\mathbf{v}^{(n)} - c\|_{\mathcal{H}} \leq C \frac{M}{(n+1)^2}.$$

Also as step (10) of the algorithm suggests the tuning parameter  $\rho^{(n+1)}$  is assigned the value of the previous iteration  $\rho^{(n)}$ . This value is fixed as long as the steps (9)-(11) run. Let us denote this fixed value by  $m$ . Combining these discussions we obtain

$$\sum_{i=0}^n |\rho^{(i)}| \|B\mathbf{v}^{(i)} - c\|_{\mathcal{H}} \leq m C M \sum_{i=0}^n \frac{1}{(i+1)^2},$$

which remains finite as  $n$  becomes large. Now suppose it takes  $n$  iterations where  $\epsilon_1^{(n)} > 2\delta_{\text{HS}}$ . From the  $(n+1)^{\text{th}}$  iteration when  $\epsilon_1^{(n+j)} < 2\delta_{\text{HS}}, j = 1, 2, \dots$  the upper bound becomes  $2\delta_{\text{HS}}$ . Combining we have

$$\sum_{i=0}^n |\rho^{(i)}| \|B\mathbf{v}^{(i)} - c\|_{\mathcal{H}} \leq r,$$

where

$$r = \max \left\{ \frac{\pi^2}{6} mCM, 2\delta_{\text{HS}} \right\}.$$

which remains finite as  $n \rightarrow \infty$ . Since  $S(t)$  is a contraction we observe that as  $n \rightarrow \infty$  the series of operators in the first term of (28) converges to  $(I - S(t))^{-1}$  which is a bounded operator. Thus we have  $\|(I - S(t))^{-1}d^{(0)}\| \leq M_1\|d^{(0)}\|$ . Hence in the limiting case we have

$$\|\lambda_1^{(n+1)} - \lambda_1^{(0)}\|_{\mathcal{H}} \leq 2M_1\|f\|_{L^\infty}\|d^{(0)}\|_{\mathcal{H}} + r$$

which is finite. This shows the convergence of the multipliers  $\lambda_1^{(n)}$ .  $\square$

## 4 Implementations and Results

### 4.1 Experiments on PIV Dataset

We first tested our algorithm on the Oseen vortex pair and compared our results with the continuity equation model. The Oseen vortex pair is a synthetic PIV sequence of dimension  $500 \times 500$ . The vortices are placed centered at the positions  $(166.7, 250)$  and  $(333.3, 250)$ . The circumferential velocity is given by  $v_\theta = (\Gamma/2\pi r)[1 - \exp(-r^2/r_0^2)]$  with the vortex strength  $\Gamma = \pm 7000$  pixels<sup>2</sup>/s and vortex core radius  $r_0 = 15$  pixels. For more details see [17].

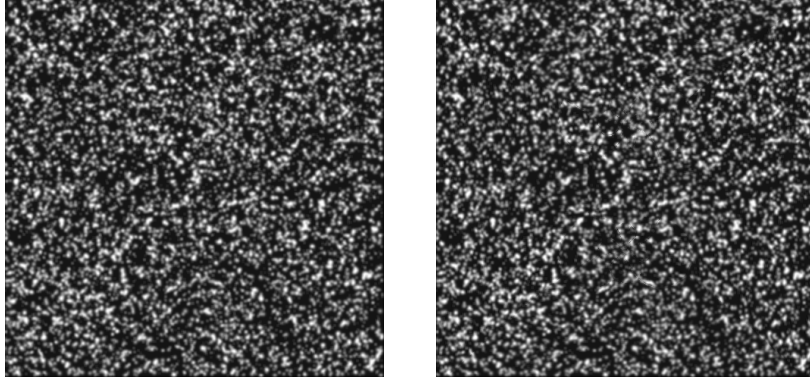


Figure 1: Oseen vortex pair



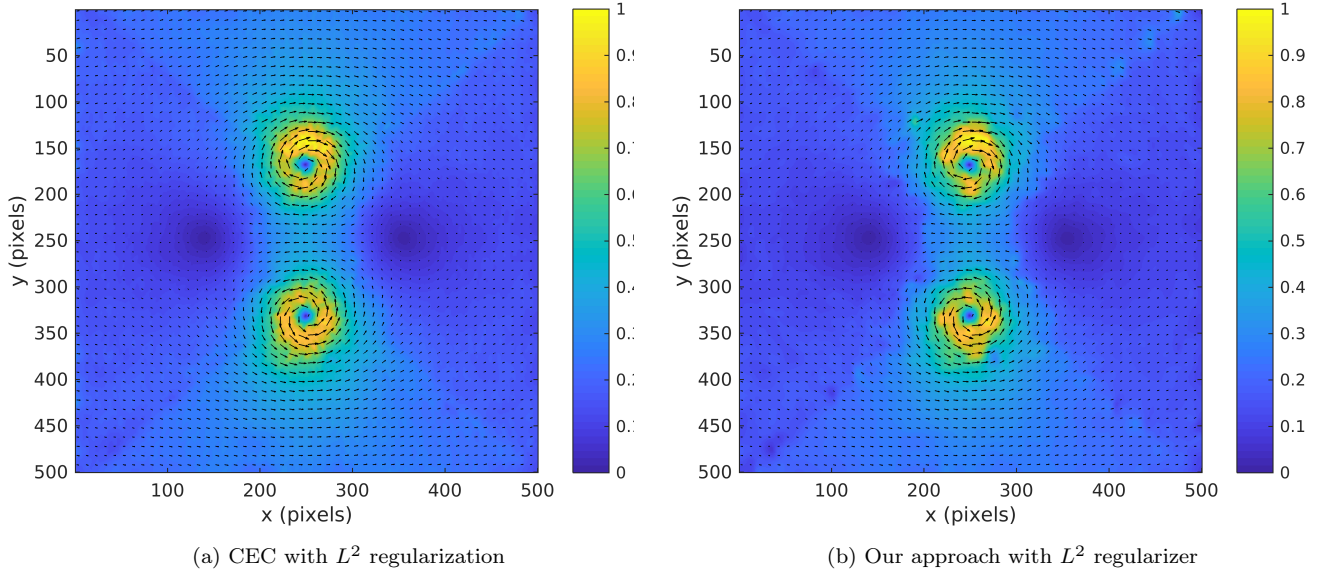


Figure 2: Velocity magnitude field of the Oseen vortex pairs

Figure (2) shows that the velocity magnitude field obtained through our constraint-based refinement algorithm is very close to the Liu-Shen continuity equation based model (CEC).

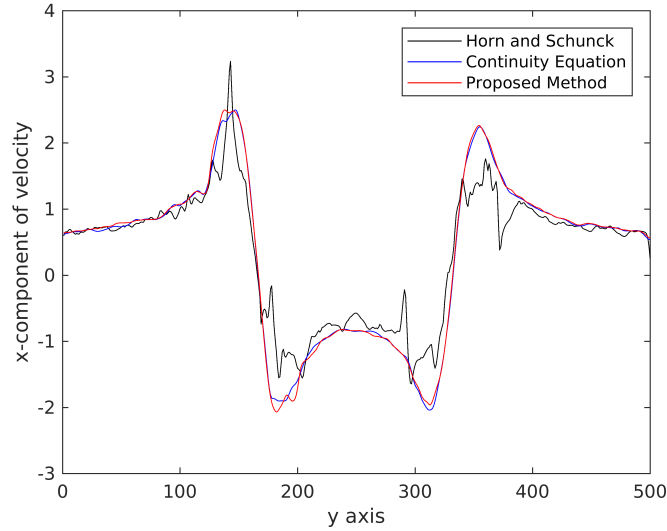


Figure 3: Distribution of the  $x$ -component of the velocity extracted from the grid images for the oseen vortex pair

Performing a similar analysis as in [24] we plot the distribution of the  $x$ -component of the velocity to obtain Figure (3). This plot compares the distribution of the  $x$ -component of the velocity extracted from the grid images for the HS model, CEC model and our constraint-based refinement model. The profiling clearly shows the closeness of our algorithm to the continuity equation based model. From the figure,

it is also seen how the Horn and Schunck model underestimates the flow components, especially near the vortex cores.

## 4.2 Experiments on Cloud Sequence

In this sequence, the movement of the fluid exhibits both formation of a vortex as well as a movement of fluid parcels. The distribution of the strength of the vortices in the cloud sequence obeys a Gaussian distribution of mean 0 and standard deviation of  $3000 \text{ (pixels)}^2/\text{s}$ .

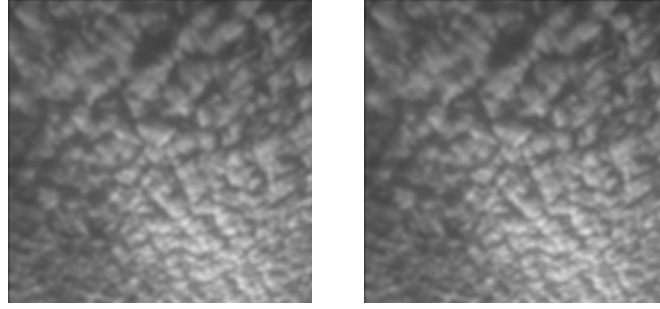


Figure 4: Cloud sequence

The comparison of the velocity magnitude plots are shown below:

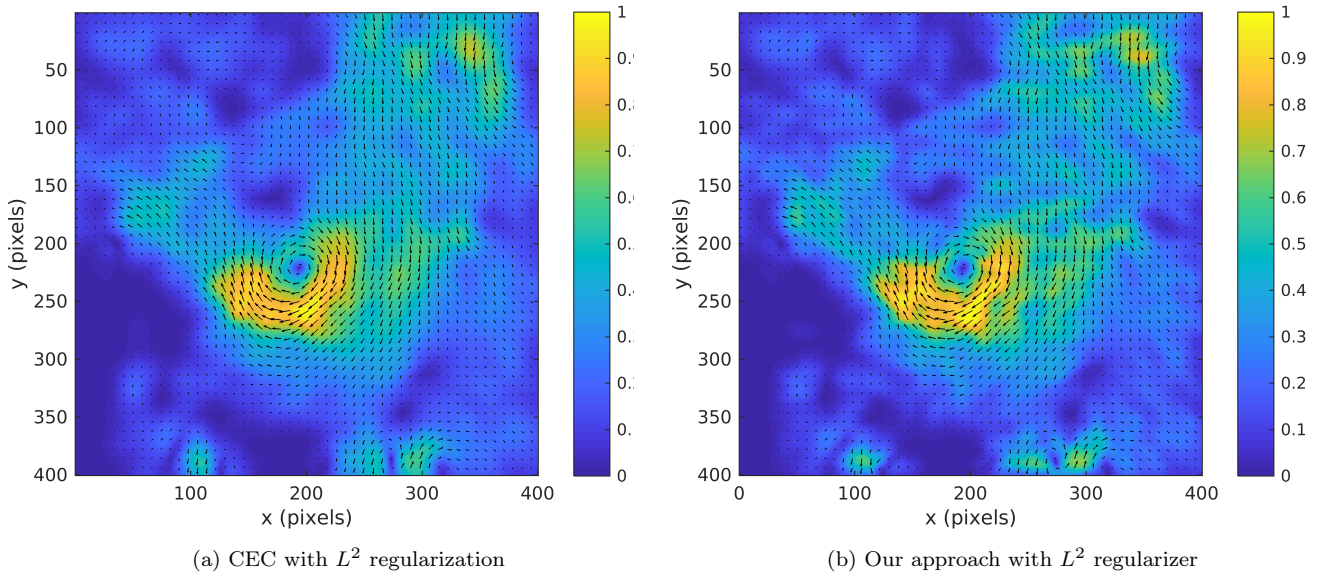


Figure 5: Velocity magnitude field of the Cloud sequence

As seen from Figure (5) the isotropic behaviour of the regularization is seen more on the continuity equation based implementation because of the denseness of the flow. Also by increasing the number of iterations we have observed that the effect of diffusion makes the vortices completely circular. The distribution of the

$x$ -component of the velocity for the cloud sequence is shown below. The Horn and Schunck estimator tends to over estimate at the peaks.

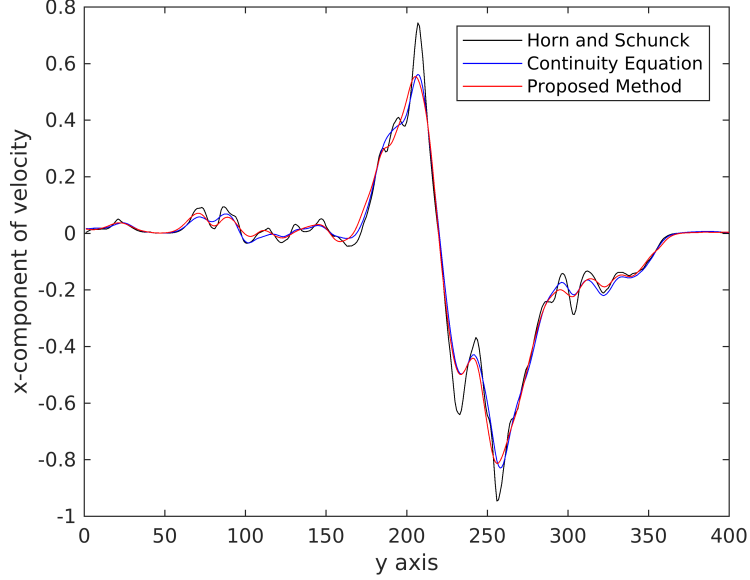


Figure 6: Comparison between the distributions of the  $x$ -component of the velocity extracted from the grid images for the cloud sequence

### 4.3 Experiments on Jupiter's White Oval Sequence

Figure (7) shows Jupiter's white oval sequence. The white ovals seen in the images are distinct storms on Jupiter's atmosphere captured by NASA's Galileo spacecraft at a time-lapse of one hour, see [17].

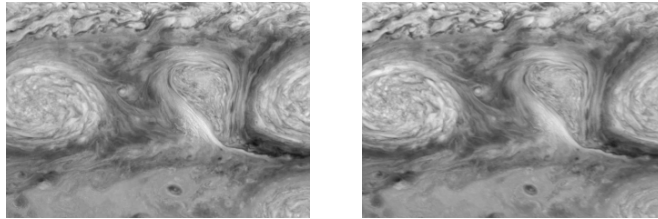
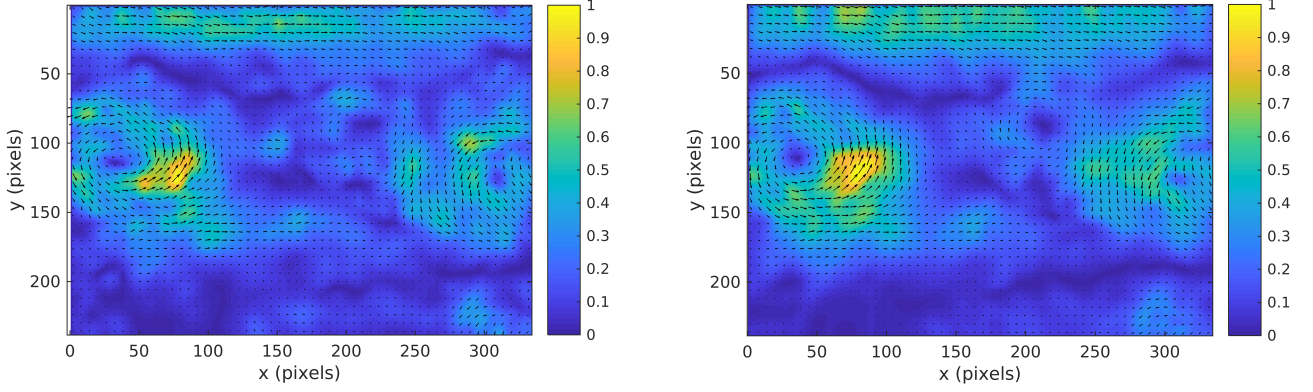


Figure 7: Jupiter's white oval sequence

#### 4.3.1 Effect of Illumination Changes on Optical Flow

Due to the time difference between adjacent frames it was observed that the sun's illumination influenced the subsequent frame considerably in a non-uniform way. To compensate the illumination effects, it is necessary to account for the illumination variation before applying the optical flow method. In the Liu-Shen implementation, an illumination correction is employed by normalizing the intensities and performing

a local intensity correction using Gaussian filters. The first plot in Figure (8) shows the results of their implementation of the CEC model.

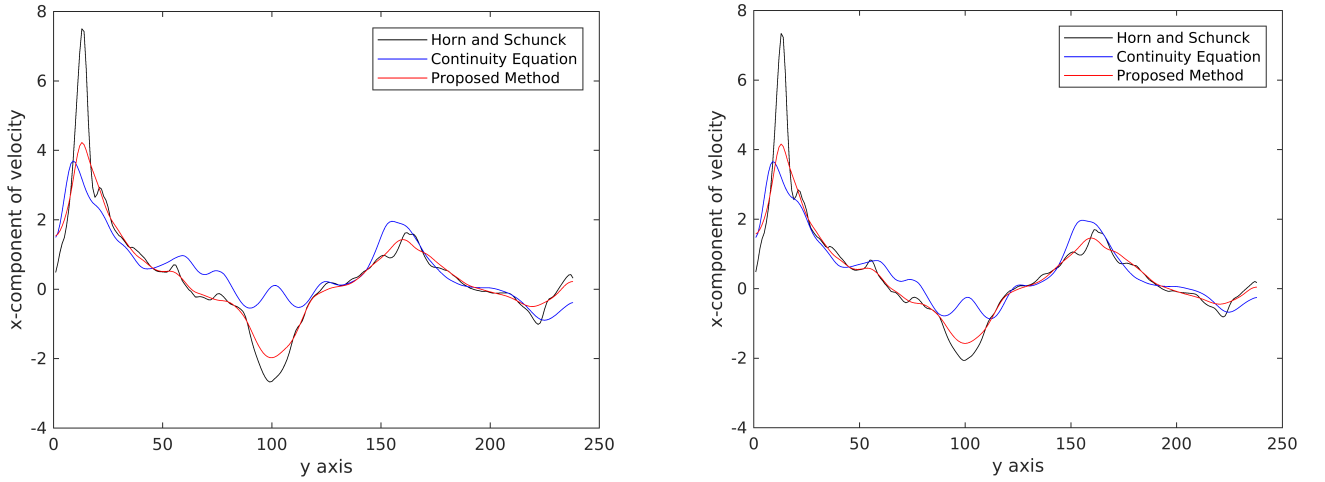


(a) CEC +  $L^2$  with illumination correction

(b) Our approach with illumination correction

Figure 8: Velocity magnitude of the Jupiter's white oval sequence

The following comparison demonstrates the effect of illumination changes on the optical flow computation.



(a) Our approach without illumination correction

(b) Our approach with illumination correction

Figure 9: Effect of the illumination correction on the distribution of the  $x$ -component of the velocity for Jupiter's white oval sequence

As seen from Figure (9) there is a large deviation near the vortex region when illumination correction is not taken into account. The deviation is minimized to a great extent as can be seen from the second image. The reason for our results (even with illumination correction) not being close to the illumination corrected CEC is because of the direct dependency of the process on the image data.

#### 4.4 Demonstration of the Flow-Driven Refinement Process

Rather than correcting the illumination changes by modifying the scheme we choose a flow-driven refinement process ( $\phi(f) = 1$ ) and perform a diffusion on the curl component. In order to achieve this, we consider the fourth case from Table (1),  $\phi(f) = 1$  and  $\psi = (\nabla_H \cdot \mathbf{u})^2$  where  $\nabla_H = (-\partial_y, \partial_x)$  is the Hamiltonian gradient. Introducing the symplectic gradient switches the roles of divergence and curl in the Equation (9) and the analysis follows in the same lines. As mentioned in Section (2.2) this particular choice captures the rotational aspects of the flow much better than its divergence counterpart.

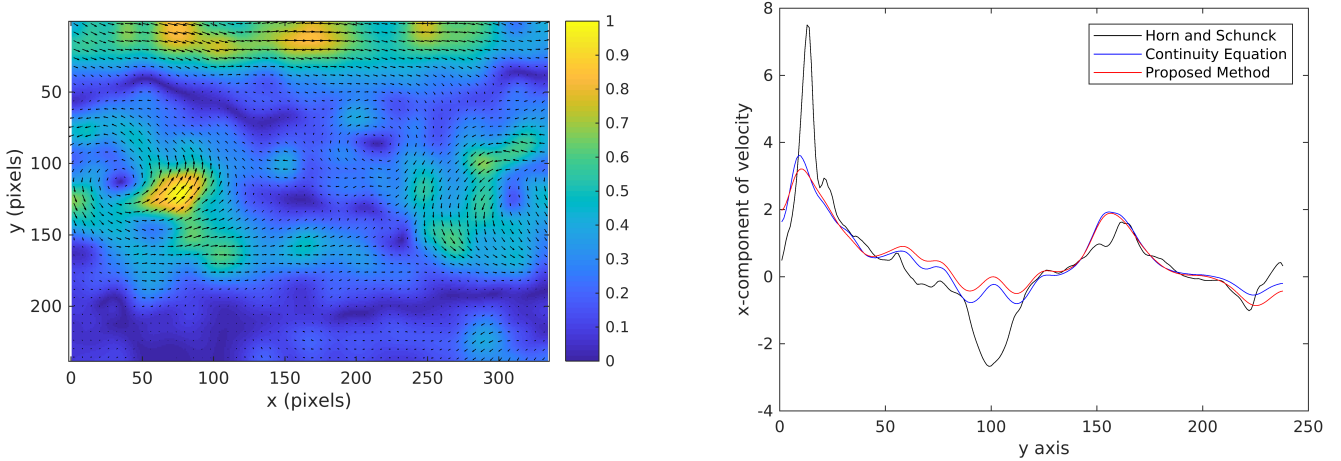


Figure 10: Plots of the Jupiter's white oval sequence with  $\phi(f) = 1$ ,  $\psi(\mathbf{u}) = (\nabla_H \cdot \mathbf{u})^2$  and without illumination correction.

Figure (10) gives the velocity magnitude plot obtained by our constraint-based refinement process  $\phi(f) = 1$  and  $\psi(\mathbf{u}) = (\nabla_H \cdot \mathbf{u})^2$  of Jupiter's white oval sequence along with the distribution of the  $x$ -component of the velocity. The ovals are clearly seen in the figure. It should be noted that the flow plots of our refinement process without illumination correction is close to the CEC with illumination correction.

#### 4.5 Discussion on the Choice of Parameters

In the Liu-Shen implementation of CEC based model, the Lagrange multiplier in the HS-estimator is chosen to be 20 and in the Liu-Shen estimator, it is fixed at 2000. They observed that for a refined velocity field it does not significantly affect the velocity profile in a range of 1000-20,000 except the peak velocity near the vortex cores in this flow. For the osen vortex pair and cloud sequence, the weight parameters  $\alpha$  and  $\beta$  in our algorithm are chosen to be 100 and 0.01 respectively. It was observed experimentally that the numerical scheme converges when the ratio  $\beta/\alpha$  is less than or equal to  $10^{-4}$ .

## Conclusion

In this work, we have proposed a general framework for fluid motion estimation using a constraint-based refinement approach. We have studied the well-posedness and the regularity of the solutions using evolutionary PDE in a Hilbert space setting. We have also shown the decoupling of our system by the Cauchy-Riemann operator which leads to a diffusion process on the curl and the divergence leading to a multiplicative perturbation of the laplacian of the divergence. For a particular choice of additional constraint, we have shown that our model closely approximates the continuity equation based model by a modified augmented Lagrangian approach. Finally, we have shown the results of our algorithm on different datasets. We have also compared and shown the effect of the image data term on the refinement process by considering two different additional constraints.

## Acknowledgements

We express our deep sense of gratitude to Bhagawan Sri Sathya Sai Baba, Revered Founder Chancellor, SSSIHL. We would like to thank Dr. Shailesh Srivastava for his insight into obtaining the velocity plots.

## References

- [1] L. Alvarez, J. Esclari n, M. Lefebure, J. S nchez, “A PDE model for computing optical flow”, *Proc. XVI Congreso de Ecuaciones Diferenciales y Aplicaciones*, 1349-1356, 1999.
- [2] P. Altomare, S. Milella, G. Musceo, “Multiplicative Perturbation of the Laplacian and related Approximation Problems”, *Journal of Evolution Equations*, 771-792, 2011.
- [3] G. Aubert, R. Deriche, P. Kornprobst, “Computing Optical Flow via Variational Techniques”, *SIAM Journal of Applied Mathematics*, 60:156-182, 1999.
- [4] G. Aubert, P. Kornprobst, *Mathematical Problems in Image Processing, Calculus of Variations and Partial Differential Equations*, Springer, 2002.
- [5] H. Brezis, *Functional Analysis, Sobolev Spaces and Partial Differential Equations*, Springer, 2011.
- [6] X. Chen, P. Zill , L. Shao, T. Corpetti, “Optical Flow for Incompressible Turbulence Motion Estimation”, *Experiments in Fluids*, 56:8, 2015.
- [7] T. Corpetti, E. M min, P. P rez, “Estimating Fluid Optical Flow”, *Proceedings of the 15th International Conference on Pattern Recognition*, 3:1033-1036, 2000.

- [8] T. Corpetti, D. Heitz, G. Arroyo, E. Mémin, A. Santa-Cruz, “Fluid Experimental Flow Estimation based on an Optical Flow Scheme”, *Experiments in Fluids*, 40:80-97, 2006.
- [9] B. Dacorogna, *Direct Methods in Calculus of Variations*, Springer, 2008.
- [10] P. Darko, “On  $L^p$  Sobolev Space Estimates for the Inhomogeneous Cauchy-Riemann Equation on Polycylinders”, *Complex Variables*, 38:367-373, 1999.
- [11] P. Eidus, “The Perturbed Laplace Operator in a weighted  $L^2$  space”, *Journal of Functional Analysis*, 100:400-410, 1991.
- [12] L.C. Evans, *Partial Differential Equations*, Second Edition, Americal Mathematical Society, 2010.
- [13] R. Glowinski, P. Le Tallec, *Augmented Lagrangian and Operator-Splitting Methods in Nonlinear Mechanics*, SIAM, 1989.
- [14] D. Heitz, E. Mémin, C. Schnörr, “Variational Fluid Flow measurements from Image Sequences: Synopsis and Perspectives”, *Experiments in Fluids*, 48:369-393, 2010.
- [15] W. Hinterberger, O. Scherzer, C. Schnörr, J. Weickert, “Analysis of Optical Flow Models in the Framework of Calculus of Variations”, *Numer. Funct. Anal. and Optimiz.*, 23(1&2):69-89, 2002.
- [16] B.K.P. Horn, B.G. Schunck, “Determining Optical Flow”, *Artificial Intelligence*, 17:185-203, 1981.
- [17] T. Liu, “OpenOpticalFlow: An Open Source Program for Extraction of Velocity Fields from Flow Visualization Images”, *Journal of Open Research Software*, 5:29, 2017.
- [18] T. Liu, L. Shen, “Fluid Flow and Optical Flow”, *Journal of Fluid Mechanics*, 614:253-291, 2008.
- [19] A. Luttmann, E.M. Bollt, R. Basnayake, S. Kramer, N.B. Tufillaro, “A Framework for Estimating Potential Fluid Flow from Digital Imagery”, *Chaos: An Interdisciplinary Journal of Nonlinear Science*, 23:3, 2013.
- [20] J. Nocedal, J. Wright Stephen, *Numerical Optimization*, 2nd Edition, Springer, 2006.
- [21] G. Sapiro, *Geometric Partial Differential Equations and Image Analysis*, Cambridge University Press, 2001.
- [22] C. Schnörr, “Determining Optical Flow for Irregular Domains by Minimizing Quadratic Functionals of a Certain Class”, *International Journal of Computer Vision*, 6:25-38, 1991.

- [23] E. Vold, L. Yin, W. Taitano, K. Molvig, B. Albright, “Diffusion-driven Fluid Dynamics in Ideal Gases and Plasmas”, *Physics of Plasmas*, 25(6), 062102, 2018.
- [24] B. Wang, Z. Cai, L. Shen, T. Liu, “An Analysis of Physics-based Optical Flow”, *Journal of Computational and Applied Mathematics*, 276:62-80, 2015.
- [25] J. Weickert, C. Schnörr, “A Theoretical Framework for Convex Regularizers in PDE-based Computation of Image Motion”, *International Journal of Computer Vision*, 45:245-264, 2001.
- [26] R.P. Wildes, M.J. Amabile, A. Lanzillotto, T. Leu, “Recovering Estimates of Fluid Flow from Image Sequence Data”, *Computer Vision and Image Understanding*, 80:246-266, 2000.